Results in Chemistry xxx (xxxx) 101045

Contents lists available at ScienceDirect

Results in Chemistry

journal homepage: www.elsevier.com

Journal Cover Image

pH variation in protic and pseudo-protic ionic liquid–water solutions

Hiroshi Abe *, Taichi Ohkubo, Taiki Miike

Department of Materials Science and Engineering, National Defense Academy, 1-10-20 Hashirimizu, Yokosuka 239-8686, Japan

ARTICLE INFO

Keywords:
Protic ionic liquid
Pseudo-protic ionic liquid
On-proton/off-proton
pH variety of ionic liquid–water solutions

ABSTRACT

In this study, the proton behaviors of protic ionic liquid (pIL) and pseudo-protic ionic liquid (psIL)–water solutions were investigated using pH measurements. Propylammonium nitrate (PAN) as a representative pIL was characterized based on the water concentration dependence of the pH values. Above 60 mol% H_2O, pH increased by increasing the water concentration. Furthermore, 1-ethylimidazolium nitrate [C_2Him][NO_3] as a psIL was a weakly acidic. The pH values of [C_2Him][NO_3]–H_2O were not affected by the water content. Two different pIL and psIL provided different proton behaviors in the water-mediated circumstance.

1. Introduction

Ionic liquids (ILs) are electrochemically stable and have been used in electrochemical applications [1–5]. The ILs are classified into aprotic ionic liquids (apILs) and protic ionic liquids (pILs) [6]. Particularly, the pILs were distinguished by introducing the difference in pK_a value, ΔpK_a [7–10]. Regarding ΔpK_a, ionicity was quantified using diffusion coefficients and determined by pulsed-gradient spin-echo NMR [11–16]. Furthermore, ionicity was modified using the effective cation and anion sizes [14].

The hydrogen-bonding network of the pILs was examined using density functional theory (DFT) calculations and Raman spectroscopy [17]. The pILs reported were ethylammonium nitrate, EAN, propylammonium nitrate, PAN, and butylammonium nitrate. Hydrogen bonding were derived from O–H···N → O^-···H–N^+. Using NMR spectroscopy, hydrogen bond dynamics of the pILs was examined combined with DFT [18,19]. Strong hydrogen bonds appeared in the pILs. Conversely, "pseudo-protic ionic liquid (psIL)" was discovered, and was defined in the previous paper [20]. The psIL evaluated was 1-methylimidazolium acetate, [C_1Him][OAc], which has low ΔpK_a. Moreover, the proton dynamics of [C_1Him][OAc] was also investigated using molecular dynamics (MD) simulations [21]. The high ionic conductivity of [C_1Him][OAc] was explained by Grotthuss-like proton conduction. Additionally, the electrochemical properties were examined using deuterated acetate [22].

Proton anomalies in ILs were enhanced by water additives. For instance, as an apIL, rhythmic pH oscillations appeared with the lapse of time in *N*,*N*-diethyl-*N*-methyl-*N*-(2-methoxyethyl)ammonium tetrafluoroborate, [DEME][BF_4], and water system [23–25]. Despite the same apILs, an entirely different pH behavior was observed in the imidazolium IL–water system. The water concentration dependence of pH was observed using 1-butyl-3-methylimidazolium tetrafluoroborate, [C_4mim][BF_4], and the water system [26]. However, no pH oscillation was observed for [C_4mim][BF_4]–water [24]. Pure EAN was acidic because of the strong hydrogen bonding [27,28]. Low-temperature crystal polymorphs and multiple pathways of pure EAN [29] and PAN [30] supported the proton-induced anomalies. Moreover, EAN–H_2O provided distinct rhythmic fluctuations of pH in the water-rich region [28].

In this study, we investigated pH of the water-mediated pIL and psILs. Two different types of pIL and psILs demonstrated entirely different proton behaviors in the water-mediated circumstance. pH in the psILs was not influenced by the water concentration.

2. Materials and methods

2.1. Materials

Hydrophilic PAN (99.9%), [C_1Him][NO_3] (99.8%), and 1-ethylimidazolium nitrate [C_2Him][NO_3] (99.9%) were obtained from IoLiTec, Co. [C_2Him][NO_3] is also regarded as the psIL in the same manner with [C_1Him][NO_3]. Vacuum drying was carried out for a week using a diaphragm type dry vacuum pump (DTU-20. ULVAC Co.), where a clean vacuum state was obtained without contaminations. Distilled water (Kanto Chemical Co.) was used for water additive.

Molecular structures of the pIL and psILs are shown in Fig. 1. Because the pIL and psILs are hydrophilic, the pIL and psILs were mixed with water under a helium purge in a glove box to exclude atmospheric humidity.

* Corresponding author.
E-mail address: ab@nda.ac.jp (H. Abe).

https://doi.org/10.1016/j.rechem.2023.101045
Received 3 July 2023; Accepted 19 July 2023
2211-7156/

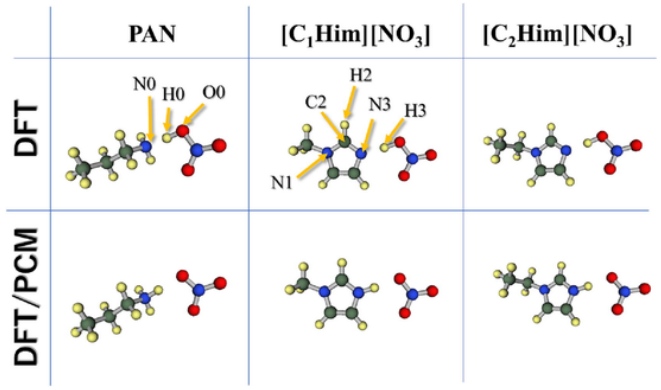

Fig. 1. Molecular structures of PAN, $[C_1Him][NO_3]$, and $[C_2Him][NO_3]$, calculated by DFT and DFT/PCM. N0, H0, O0, N1, C2, H2, N3, and H3 represent the atomic descriptions of the $[C_nHim]^+$ cations. Hydrogen positions are varied depending on the calculation types (see text).

2.2. Phase diagram determinations

The phase diagram of the psIL and water mixtures was obtained by the visual cloud-point determinations [31,32]. The mixtures were cooled from 80 °C to −80 °C using a conventional water bath and ethanol bath (Yamato Scientific Co., BE200). The temperature was monitored by a Pt100 (Netsushin Co.), and the cooling rate was 1.5 °C/min.

2.3. pH measurements

For pH measurements, a semiconductor pH sensor (ISFET 0040-10D, Horiba Co.) was used. The pH values were calibrated using standard pH solutions: $KH_3(C_2O_4)_2{\cdot}2H_2O$ (pH = 1.68), $C_6H_4(COOK)(COOH)$ (pH = 4.01), and $KH_2PO_4 + Na_2HPO_4$ (pH = 6.86) (Horiba Co.). The semiconductor pH meter was placed in a metal container continuously flushed with helium gas to reduce atmospheric moisture [28]. Inside the container, the pH sensor was immersed in the sample. Every 2 s, the pH values were stored in a computer by fixing temperature (5 °C). An ethanol bath (BB301, Yamato Scientific Co.) was used for the pH measurements to control the temperature within 0.1 °C.

2.4. Density functional theory calculations

DFT calculations were performed to investigate the interaction among cations, anions, and water molecules. Proton shifting of the optimized molecular complex was visualized by DFT. The proton shifting was changed by the water molecule. All DFT calculations were performed using the Lee–Yang–Parr correlation (B3LYP) 6–31 + + G(d, p) basis set [33,34] and the *Firefly* (PC-GAMESS) package [35,36]. The solvation effects were investigated by the polarized continuum model (PCM) [37]. In the PCM, a cavity surrounded by solvent and a continuum dielectric medium is assumed, and the solute is placed in the cavity. In addition, natural bond orbital (NBO) population analysis can estimate atomic charges in molecules [38]. Donor-acceptor behaviors were demonstrated using the NBO analysis (NBO 7.0.10). In this study, the PCM and NBO calculations with water as solvent were carried out.

3. Results and discussion

3.1. Water concentration dependence of pH in the PAN–water system

The liquid structures of EAN–H_2O and PAN–H_2O were determined by small- and wide-angle X-ray scattering (SWAXS) [39]. In the SWAXS patterns of pure systems, the pre-peak position of PAN, indicating that a larger nano-heterogeneity was developed in PAN. Moreover, the pre-peak position of EAN–H_2O was nearly constant over the entire region of water concentration, while that of PAN–H_2O changed depending on the water concentration. In fact, the pre-peak shifting of PAN–H_2O was induced above 60 mol%. On the mesoscopic scale, the molecular correlations and proton network of EAN were not affected in any water concentrations, while the water additive in PAN disturbed the nano-heterogeneity of the mixtures in the water rich region.

pH values of PAN–H_2O at 5 °C were plotted on the water concentration scale (Fig. 2). The water concentration dependence of pH in PAN–H_2O resembled that in EAN–H_2O [28]. Below 50 mol%, the pH of PAN–H_2O was nearly constant, although an increment of pH occurred at 60 mol%. Above 90 mol%, a drastic increasing pH to neutral was predominantly observed by increasing the water concentration. The proton behavior of PAN–H_2O was separated in three water concentration regions: (i) $x < 60$ mol%, constant pH, (ii) $60 < x < 90$ mol%, gradual increasing pH, and (iii) 90 mol% $< x$, rapid increment of pH. The pH in the regions (ii) and (iii) corresponds to the pre-peak shifting on the SWAXS patterns [39]. Therefore, the proton behavior in PAN–H_2O is related to the nano-heterogeneity. The pH values of PAN–H_2O were lower than those of EAN–H_2O. In the PAN–H_2O, the protons are located preferentially around the $[NO_3]^-$ anions (Fig. 1).

To understand the pH variation in the IL–water solutions, DFT and DFT/PCM simulations were performed. By NBO analyses, nitrogen atom changes from −0.5501*e* (ion pair) to −0.7162*e* (transition state) indicated the hydrogen bonding states in acetate-based pILs [40]. By NBO analyses, nitrogen atom changes from −0.5501e (ion pair) to −0.7162e (transition state) indicated the hydrogen bonding states in acetate-based pILs [40]. Using NBO population analysis, the calculation results in EAN, PAN, and their water complexes are obtained as shown in Fig. S1. In both systems, they are stabilized by water media of DFT/PCM. Focusing on the NBO charge of nitrogen of the cations, the calculated N charge in the pure PAN cation is −0.898*e* (transition state), while that in the pure EAN cation is −0.902*e* (transition state). More importantly, in the water media (DFT/PCM), the N charge in the PAN cation changes to −0.789*e* (ion pair). Focusing on PAN in DFT and DFT/PCM (Fig. S1), C_3H_7-NH_2 (off-proton) and C_3H_7-NH_3^+ (on-proton) correspond to transition state and ion pair, respectively. Compared with other atoms, the NBO charge of nitrogen of the cations is directly connected with acidic or neutral in the pIL-water system.

3.2. Water concentration dependences of pH in $[C_1Him][NO_3]$– and $[C_2Him][NO_3]$–water systems

Fig. 3 displays the phase diagrams of $[C_1Him][NO_3]$– and $[C_2Him][NO_3]$–H_2O. At room temperature, pure $[C_1Him][NO_3]$ is in solid state. Crystallization temperature of pure $[C_1Him][NO_3]$ was 66 °C. With increasing water concentration, the crystallization temperatures of $[C_1Him][NO_3]$–H_2O decreased gradually (Fig. 3). The minimum crystallization temperature appeared at 80 mol%. Above 80 mol%, the crystallization temperatures became higher. Below 50 mol%, $[C_1Him][NO_3]$–H_2O was a solid state at room temperature. Thus, at room temperature, the pH values in the liquid state were observable above 60.0 mol%. On the other hand, pure $[C_2Him][NO_3]$ having a longer alkyl chain crystallized at −3.8 °C. The minimum crystallization temperature in $[C_2Him][NO_3]$–*x* mol% H_2O was found to be −75 °C (Fig. 3). In $[C_2Him][NO_3]$–H_2O, crystallization was not observed above 5 °C (Fig. 3); therefore, the pH could be measured at 5 °C over the entire water concentration. Furthermore, phase diagrams in Fig. 3 indicate ion pairing on the water-mediate circumstance. Compared with $[C_1Him][NO_3]$–H_2O, the ion pairing strength between the cation and anion became weaker in $[C_2Him][NO_3]$–H_2O.

To compare the pH values of $[C_nHim][NO_3]$–H_2O (n = 1 and 2), the pH values are exhibited in Fig. 4. In $[C_nHim][NO_3]$–*x* mol% H_2O (n = 1 and 2), the pH values as a function of x were measured at 5 °C. In $[C_1Him][NO_3]$–H_2O, pH indicated weakly acidic (pH = 3.1–3.2). In

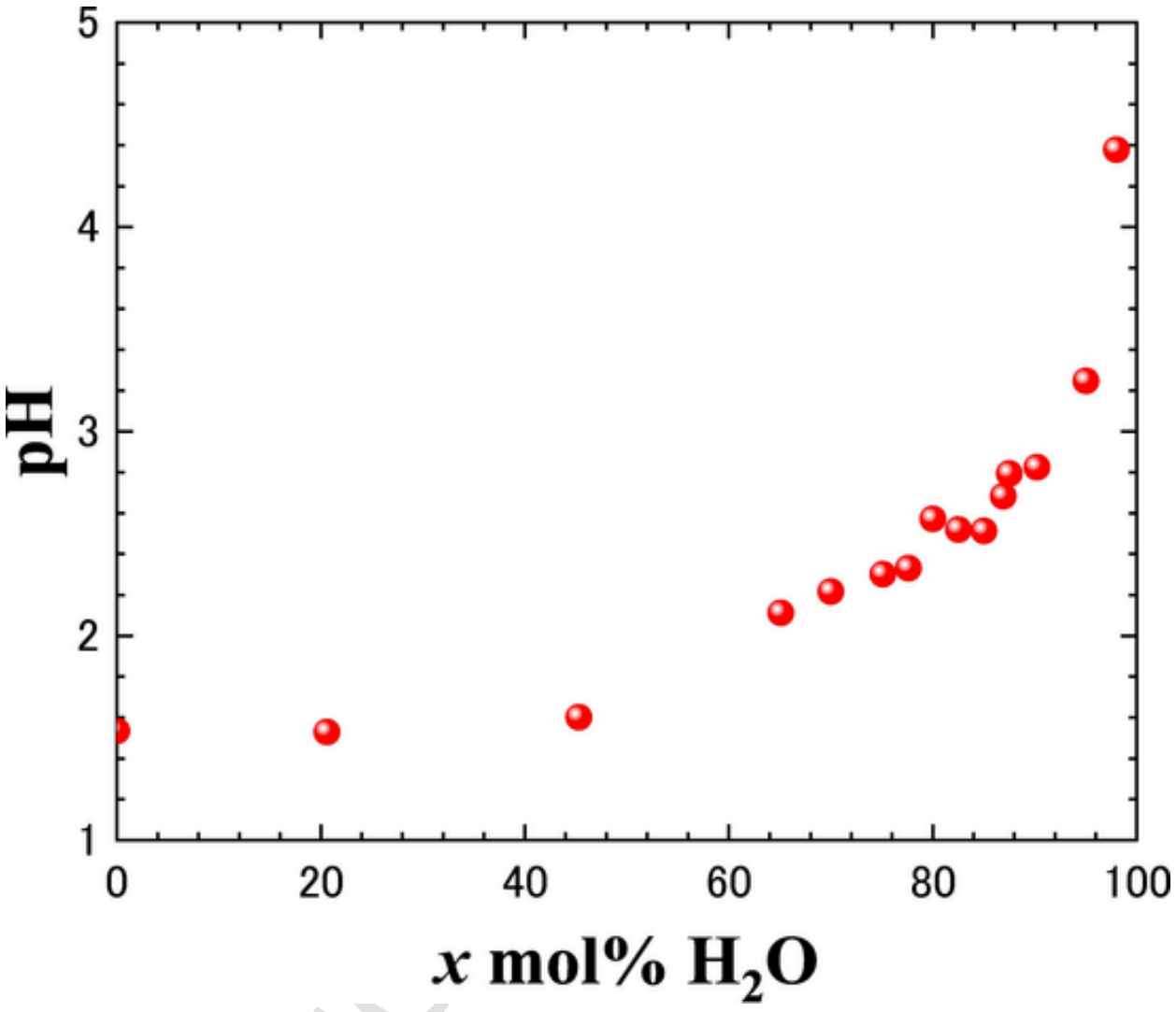

Fig. 2. Water concentration dependence of pH in the PAN–H_2O system at 5 °C. The observed pH values changed in the water-rich region.

contrast, the pH values of [C_2Him][NO_3]–H_2O were close to neutral. Therefore, it is deduced that the alkyl chain length of cations contributes to proton activity relating with the "superionic" behavior of the psILs. Next, we focus the pH-invariant on the *x* scale (Fig. 4). This tendency of concentration-invariant pH was not observed in other [C_4mim][BF_4] [26], [DEME][BF_4] [23], and EAN [28] (Fig. 6). This means that the proton state of the psILs is not influenced by the coordination numbers of the water molecules. Considering little water concentration dependences of the psILs in Fig. 4, the intrinsic proton behaviors [20,22] of the psILs could not be influenced by the water circumstances. The *x* mol%-invariant pH of the psILs could be connected with the "superionic" behavior, which is explained by Markov chain models [41]. Markov chains are stochastic models, describing possible events of the reacting species.

3.3. Time dependences of pH in pIL and psILs

Time dependences of pH in PAN–80.0 mol% H_2O were measured at a fixed temperature (Fig. 5(a)). The temperature was set to be 5 °C to reduce the thermal effect. Pure PAN crystallized at −36 °C (T_{C1}) [30]; therefore, at 5 °C, PAN–80.0 mol% H_2O cannot freeze at all. When the temperature reached 5 °C, time started to be counted. Compared with the EAN–*x* mol% H_2O system [28], the rhythmic pH oscillations were suppressed in PAN–80.0 mol% H_2O (Fig. 5(a)). Here, we predict the different time dependences between EAN- and PAN-water systems from a viewpoint from their nano-heterogeneities in the water-rich region [39]. The pre-peak position of EAN–H_2O was nearly constant over the entire region of water concentration, while that of PAN–H_2O changed depending on the water concentration. In fact, the pre-peak shifting of PAN–H_2O was induced above 60 mol%. On the mesoscopic scale, the specific proton network in PAN–H_2O was disturbed by the nano-heterogeneity of the mixtures in the water rich region. Therefore, the rhythmic pH oscillation was not induced in PAN-H_2O.

Fig. 5(b) and 5(c) displays time dependences of pH in [C_1Him][NO_3]–80.0 mol% H_2O and [C_2Him][NO_3]–80.0 mol% H_2O, respectively. The mixtures were a liquid state at 5 °C (Fig. 3). Rhythmic pH oscillations were not observed for [C_1Him][NO_3]–H_2O and [C_2Him][NO_3]–H_2O. The time-invariant pH indicates that the mixtures are equilibrated at the early stage. Since the pH oscillations in EAN-H_2O [28] were suppressed in [C_1Him][NO_3]–H_2O and [C_2Him][NO_3]–H_2O, the specific proton fluctuations among the molecules did not occur in the psILs.

3.4. pH variation in apIL–, pIL–, and psIL–water systems

Hydrophilic [C_4mim][BF_4] as an apIL is well resolved in water. The pH values of [C_4mim][BF_4]–H_2O have been previously reported [26]. The water concentration dependence of pH in [C_4mim][BF_4]–H_2O is

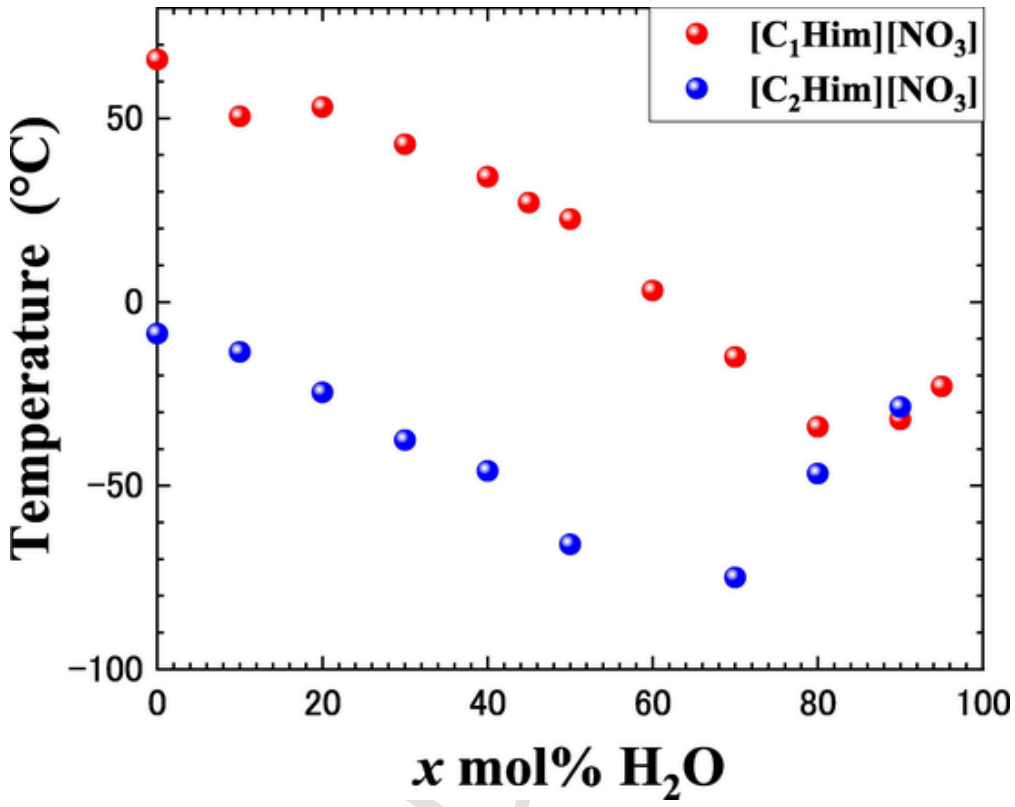

Fig. 3. Phase diagrams of $[C_1Him][NO_3]$– and $[C_2Him][NO_3]$–H_2O. Crystallization temperatures of $[C_1Him][NO_3]$ were higher than those of $[C_2Him][NO_3]$.

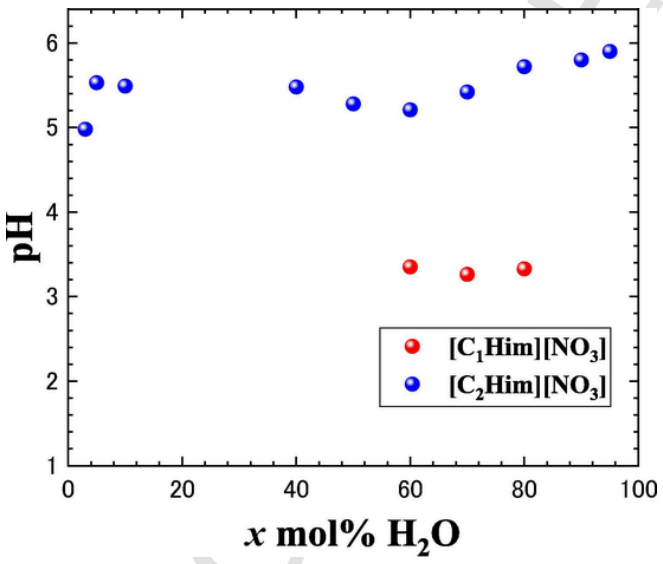

Fig. 4. Water concentration dependences of pH in the $[C_1Him][NO_3]$– and $[C_2Him][NO_3]$–H_2O systems (5 °C). The pH values were almost constant on the water concentration.

schematically illustrated in Fig. 6. Pure $[C_4mim][BF_4]$ exhibited strong acidity. When $[C_4mim][BF_4]$ was diluted gradually with water, the pH became weakly acidic. Once the pH reached 3.5, a constant pH was observed up to 90 wt% H_2O (99.1 mol% H_2O). Above 90 wt% H_2O, the pH drastically increased up to 7. Regarding water concentration, the pH of $[C_4mim][BF_4]$–H_2O was divided into three regions (Fig. 6). Conversely, no rhythmic pH oscillation was observed for $[C_2mim][BF_4]$ –90 mol% H_2O and $[C_4mim][BF_4]$–90 mol% H_2O [24]. In contrast, $[DEME][BF_4]$ as another apIL provided the water-induced complex pH behaviors (Fig. 6) [24]. The $[DEME]^+$ cation possesses the ether bond, which is an electronegative part [41]. Furthermore, pure $[DEME][BF_4]$ was found to be weakly acidic. More importantly, in the water-poor region, the pH shifted to the base region. However, above 50 mol%, the pH became gradually acidic and the minimum value of pH appeared at 90 mol%. As shown in Fig. 6, the pH of $[DEME][BF_4]$–H_2O was sensitive to the water concentration. Molecular aggregations could be modified by the coordination number of water molecules. Moreover, rhythmic pH oscillations were observed in the water-rich region [24]. One possible reason is that the $[DEME]^+$ cation has a proton capture site, which is the ether bond. Because the $[BF_4]^-$ anion can also capture protons, a proton in the water-mediated circumstance could fluctuate between cation and anion. Both on time and water concentration scales, the complex pH behaviors of $[DEME][BF_4]$–H_2O were derived from the proton fluctuations, which are activated by the water additive.

PAN is a typical pIL, which is strongly acidic. Despite water dilution, the strong acidic feature was maintained up to 50 mol% (Fig. 2). The water additive cannot disturb the proton activity in PAN–H_2O mixtures below 50 mol%. At 60–90 mol%, the pH value of PAN–H_2O gradually increased as a crossover of pIL-like with water-like regimes. Above 90 mol%, the protic circumstance collapsed, and the pH value shifted drastically up to 7. In contrast, psILs exhibited an entirely different water concentration dependence of pH (Fig. 4). For instance, pure $[C_2Him][NO_3]$ exhibited pH ~ 5. Over the entire water concentration, $[C_2Him][NO_3]$–H_2O was nearly neutral (pH = 5–6). As mentioned, for pure $[C_1Him][OAc]$ [20], neutral molecules in psIL are related to fast proton conduction, which is explained by the Grotthuss mechanism. The Grotthuss mechanism is known as a proton jumping model. The model was introduced to explain high diffusion rate of the proton under an electric field.

3.5. Ab initio calculations in pIL– and psIL–water systems

Hydrogen bonding was expressed by the bonding length between the atoms. As shown in Fig. 1, the hydrogen bonding states were en-

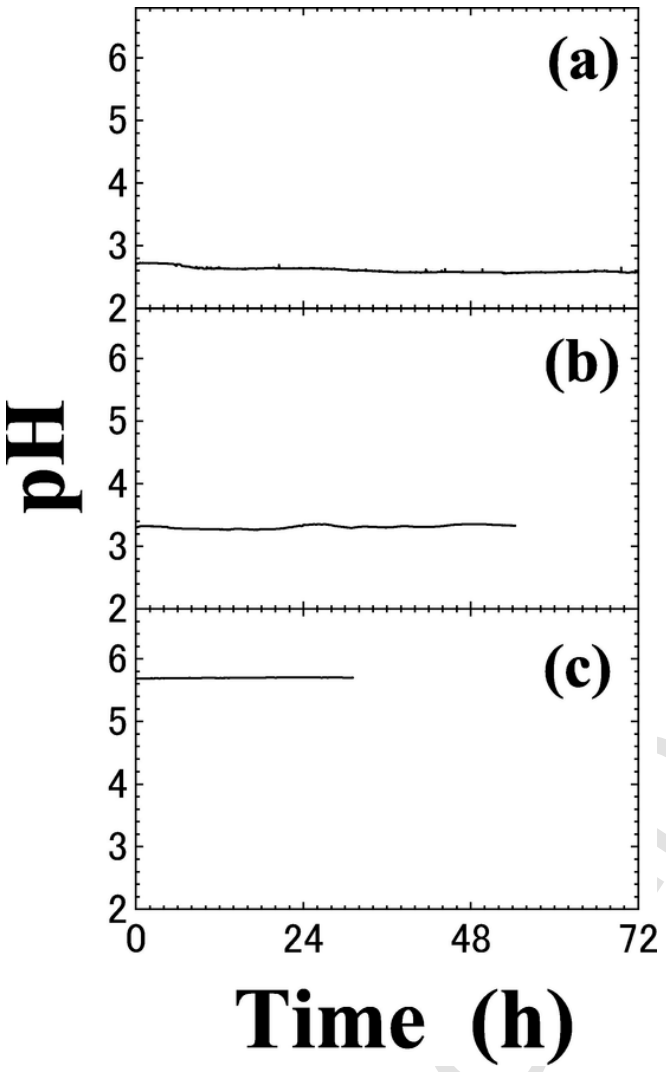

Fig. 5. Time evolution of pH for (a) PAN–80.0 mol% H_2O, (b) $[C_1Him][NO_3]$ –80.0 mol% H_2O, and (c) $[C_2Him][NO_3]$–80.0 mol% H_2O by fixing temperature (5 °C). Just after reaching 5 °C, the time was counted. pH fluctuations as seen in EAN-H_2O [28] were not observed on the time scale. Time-invariant pH values suggest that the mixtures were equilibrated at the early stage.

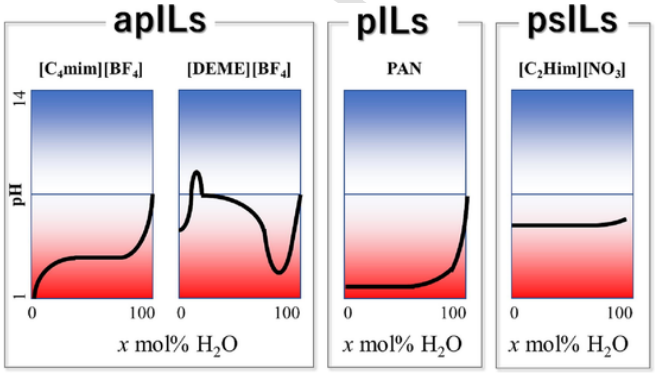

Fig. 6. Schematic representing water concentration dependences of pH. Water-driven pH variation of the apIL–, pIL–, and psIL–water systems. $[DEME][BF_4]$–H_2O indicates the complicated water concentration dependence of pH. The pH values of psILs were almost constant on the water concentration.

tirely different at each other. Conventional DFT calculations suggest a pure system without water. Solvation effect is taken into account in PCM. Therefore, in DFT/PCM, calculation results indicate molecular interactions in the water-rich region. By the geometrical relations of the optimized molecular structures using DFT and DFT/PCM, we estimated hydrogen bonding nature in the pIL–, and psIL–water systems.

For instance, the DFT and DFT/PCM calculations in the PAN–water system predicted the bonding distances of N0···H0–O0, and N0–H0···O0 (Table 1). In pure PAN, N0···H0, and H0–O0 were found to be 1.557 Å and 1.059 Å, respectively (Table 1). The NBO charge of N0 becomes −0.8980*e* (transition state) as the proton donor site. Clearly, the proton is captured by the $[NO_3]^-$ anion. The DFT calculation of pure PAN corresponds to the low pH value. When one water molecule is inserted in the DFT calculation, the water concentration is equivalent to 50 mol% H_2O. By adding the water molecule, the N0-H0 distance (1.751 Å) becomes longer. Compared with the N0–H0 distance in pure PAN (1.557 Å), the 12.5% extension was simulated in the one PAN and one H_2O system. Moreover, the NBO charge of N0 is −0.9192*e* (transition state). In contrast, the DFT/PCM surrounded by the water molecules provides no proton transfer (Table 1). The N0-H0 distance of 1.054 Å corresponds to 32.3% reduction from the N0-H0 distance in pure PAN. Furthermore, the NBO charge of −0.78992*e* (ion pair) was obtained by DFT/PCM. The short N0-H0 distance and −0.78992*e* (ion pair) are connected with the large pH values in the water-rich region.

As another pIL, triethylammonium, $[TEA]^+$, a cation-based pIL was examined by DFT and MD [18,19,43]. For [TEA][X], the anion (X) dependence of proton – acceptor distances was connected with the acidity. In the MD simulations, the molecular distances and orientational orders were analyzed.

Next, we focus the psILs using the DFT and DFT/PCM calculations. In the case of $[C_nHim]^+$ cations (n = 1 and 2), two proton capture sites are considered as shown in Fig. 7. Two proton donor sites at N3–H3 and C2–H2 are defined as Type I and Type II, respectively. Since the pH values of $[C_1Him][NO_3]$–H_2O were observed only above 60 mol% (Fig. 4), $[C_2Him][NO_3]$–H_2O is calculated for a comparison. For instance, in the DFT calculation of Type I, $[C_2im]$ without proton (off-proton) is expressed by N3···H3 of 1.567 Å, and H3–O of 1.049 Å (Table 1). In the same manner with PAN, proton of $[C_2im]$ (off-proton) shifted close to the $[NO_3]^-$ anion. Nevertheless, the NBO charge of N3 of $[C_2im]$ (-0.5552*e* as ion pair) is different extensively from that of PAN. The less negative charge of N3 implies the nearly neutral pH of pure $[C_2Him][NO_3]$. Similarly, the Type II of $[C_2Him][NO_3]$ was calculated by DFT. It should be noticed that $[C_2Him]^+$ (on-proton) is preferred in Type II (Fig. 7). Although the proton is captured by the cation, the NBO charge of N3 in Type II was evaluated to be −0.5402*e* (ion pair). Both in Type I and Type II, the NBO charges are comparable in pure $[C_2Him][NO_3]$. If we add one water molecule, the proton returns to the cation and the ionic $[C_2Him]^+$ cation with proton (on-proton) is formed. In Type I with one water molecule, the N3–H3 distance was

Table 1
Bonging lengths of hydrogen bonding in the ionic couples. N0, H0, O0, C2, H2, N3, H3, and O are provided in Fig. 1. The calculated bonding lengths depended extensively on the calculation types.

		PAN		$[C_2Him][NO_3]$			
				Type I		Type II	
		N0–H0 (Å)	H0–O0 (Å)	N3–H3 (Å)	H3–O (Å)	C2–H2 (Å)	H2–O (Å)
DFT	No water	1.557	1.059	1.567	1.049	1.118	1.718
	One water	1.751	1.029	1.125	1.415	1.094	1.945
DFT/PCM		1.054	1.726	1.048	1.708	1.088	2.113

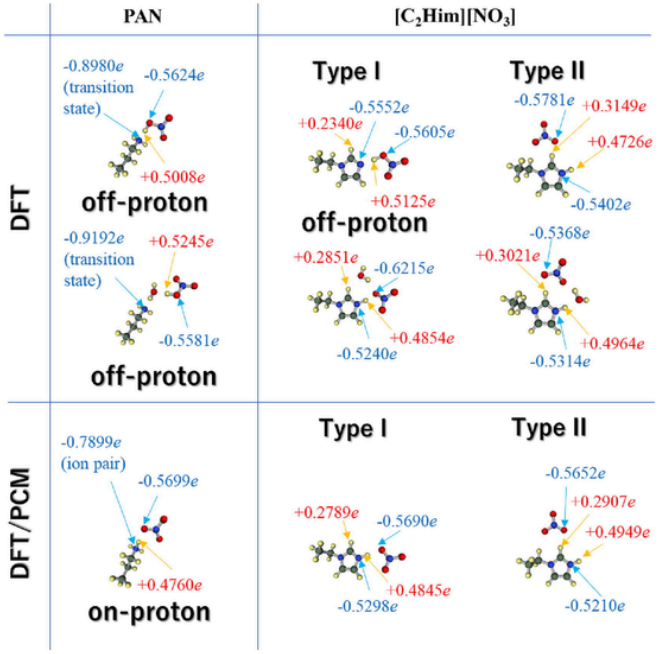

Fig. 7. DFT and DFT/PCM calculations of PAN and $[C_2Him][NO_3]$ with/without water. NBO charges are displayed in the figure. Two proton donor sites (Type I and Type 2) are considered in $[C_2Him]^+$. The NBO charges of N0 in PAN changed by the calculation types, while the NBO charges of N3 in $[C_2Him][NO_3]$ were comparable in the different calculations.

1.125 Å. 28.2% reduction from the pure $[C_2Him][NO_3]$ (1.567 Å) was induced by one water molecule. However, the NBO charges both in Type I and Type II do not change a lot (Fig. 7). This tendency also appears in the DFT/PCM calculations, which represents the behaviors in the water-rich region. In Type I and Type II, almost constant values of the N3 NBO charges in DFT and DFT/PCM can explain the *x*-invariant pH values in the $[C_2Him][NO_3]$–H_2O system (Fig. 4). Focusing on the N3–H3 distance of Type I in the DFT/PCM calculations (1.048 Å), 33.1% reduction from pure $[C_2Him][NO_3]$ (1.567 Å) was obtained. The N3–H3 distances in DFT and DFT/PCM cannot explain the water concentration-invariant pH of $[C_2Him][NO_3]$–H_2O. Therefore, the NBO charges of N3 have a relationship with the observed pH values of $[C_2Him][NO_3]$–H_2O.

Next. we focus "superionic" behavior of the psILs. Here, we predict that two possible cation states such as $[C_2im]$ (off-proton) and $[C_2Him]^+$ (on-proton) could be realized in the $[C_2Him][NO_3]$–H_2O system. The coexistence of the cationic two states causes various proton states. If the proton almost fluctuates freely among several sites, the "superionic" behavior in the psILs could be interpreted by the mixing state of Types I and II.

4. Conclusions

Water-driven proton behaviors were examined using pIL and psILs. Pure PAN is a typical pIL, and the proton activity below 50 mol% was not affected by water additives. Above 60 mol%, pH of PAN increased with increasing the water concentration. The psILs exhibited a different pH behavior on the water concentration scale. $[C_2Him][NO_3]$–H_2O was found to be weakly acidic, and the water concentration-invariant pH of $[C_2Him][NO_3]$–H_2O indicates that the proton activity was not influenced by the water additive. With including the apILs, pH as a function of water concentration categorizes the proton varieties of IL–water solutions. The proton variety of the ILs is represented on the pH as a function of water concentration. In near future, hydrogen positions in the unit cells of crystal pILs and psILs could be determined using neutron diffraction.

Uncited reference

[42].

Declaration of Competing Interest

The authors declare that they have no known competing financial interests or personal relationships that could have appeared to influence the work reported in this paper.

Acknowledgments

The authors appreciate the helpful discussion with Dr. F. Nemoto, Dr. T. Takekiyo and Professor Y. Yoshimura of the National Defense Academy.

Appendix A. Supplementary data

Supplementary data to this article can be found online at https://doi.org/10.1016/j.rechem.2023.101045.

References

[1] T.L. Greaves, C.J. Drummond, Protic ionic liquids: properties and applications, Chem. Rev. 108 (2008) 206–237.
[2] T.L. Greaves, C.J. Drummond, Protic ionic liquids: evolving structure–property relationships and expanding applications, Chem. Rev. 115 (2015) 11379–11448.
[3] T. Yasuda, M. Watanabe, Protic ionic liquids: Fuel cell applications, MRS Bull. 38 (2013) 560–566.
[4] M. Watanabe, Design and materialization of ionic liquids based on an understanding of their fundamental properties, Electrochem. 84 (9) (2016) 642–653.
[5] M. Watanabe, M.L. Thomas, S. Zhang, K. Ueno, T. Yasuda, K. Dokko, Application of ionic liquids to energy storage and conversion materials and devices, Chem. Rev. 117 (2017) 7190–7239.
[6] A.S. Amarasekara, Acidic ionic liquids, Chem. Rev. 116 (10) (2016) 6133–6183.
[7] M. Yoshizawa, W. Xu, C.A. Angell, Ionic Liquids by proton transfer: vapor pressure, conductivity, and the relevance of ΔpK_a from aqueous solutions, J. Am. Chem. Soc. 125 (2003) 15411–15419.
[8] J.-P. Belieres, C.A. Angel, Protic ionic liquids: preparation, characterization, and proton free energy level representation, J. Phys. Chem. B 111 (2007) 4926–4937.
[9] J.A. Bautista-Martinez, L. Tang, J.-P. Belieres, R. Zeller, C.A. Angell, C. Friesen, Hydrogen redox in protic ionic liquids and a direct measurement of proton thermodynamics, J. Phys. Chem. C 113 (28) (2009) 12586–12593.
[10] Y. Ansari, K. Ueno, C.A. Angell, Protic ionic liquids can be both free proton conductors and benign superacids, J. Phys. Chem. B 125 (2021) 7855–7862.
[11] A. Noda, K. Hayamizu, M. Watanabe, Pulsed-gradient spin-echo 1H and 19F NMR ionic diffusion coefficient, viscosity, and ionic conductivity of non-chloroaluminate room-temperature ionic liquids, J. Phys. Chem. B 105 (20) (2001) 4603–4610.
[12] H. Tokuda, S. Tsuzuki, M.A.B.H. Susan, K. Hayamizu, M. Watanabe, How ionic are room-temperature ionic liquids? An indicator of the physicochemical properties, J. Phys. Chem. B 110 (39) (2006) 19593–19600.
[13] K. Ueno, H. Tokuda, M. Watanabe, Ionicity in ionic liquids: correlation with ionic structure and physicochemical properties, Phys. Chem. Chem. Phys. 12 (2010) 1649–1658.
[14] D.R. MacFarlane, M. Forsyth, E.I. Izgorodina, A.P. Abbott, G. Annat, K. Fraser, On the concept of ionicity in ionic liquids, Phys. Chem. Chem. Phys. 11 (2009) 4962–4967.
[15] J. Stoimenovski, E.I. Izgorodina, D.R. MacFarlane, Ionicity and proton transfer in protic ionic liquids, Phys. Chem. Chem. Phys. 12 (2010) 10341–10347.
[16] S.K. Davidowski, F. Thompson, W. Huang, M. Hasani, S.A. Amin, C.A. Angell, J.L. Yarger, NMR characterization of ionicity and transport properties for a series of diethylmethylamine based protic ionic liquids, J. Phys. Chem. B 120 (2016) 4279–4285.
[17] E. Bodo, S. Mangialardo, F. Ramondo, F. Ceccacci, P. Postorino, Unravelling the structure of protic ionic liquids with theoretical and experimental methods: ethyl-, propyl- and butylammonium nitrate explored by Raman spectroscopy and DFT calculations, J. Phys. Chem. B 116 (2012) 13878–13888.
[18] A.E. Khudozhitkov, P. Stange, B. Golub, D. Paschek, A.G. Stepanov, D.I. Kolokolov, R. Ludwig, Characterization of doubly ionic hydrogen bonds in protic ionic liquids by NMR deuteron quadrupole coupling constants: differences to H-bonds in amides, peptides, and proteins, Angew. Chem. Int. Ed. 56 (2017) 14310–14314.
[19] A.E. Khudozhitkov, P. Stange, A.G. Stepanov, D.I. Kolokolov, R. Ludwig, Structure, hydrogen bond dynamics and phase transition in a model ionic liquid electrolyte, Phys. Chem. Chem. Phys. 24 (10) (2022) 6064–6071.
[20] H. Doi, X. Song, B. Minofar, R. Kanzaki, T. Takamuku, Y. Umebayashi, A new proton conductive liquid with no ions: pseudo-protic ionic liquids, Chem. Euro. J.

19 (2013) 11522–11526.
[21] J. Ingenmey, S. Gehrke, B. Kirchner, How to harvest grotthuss diffusion in protic ionic liquid electrolyte systems, ChemSusChem 11 (12) (2018) 1900–1910.
[22] H. Watanabe, T. Umecky, N. Arai, A. Nazet, T. Takamuku, K.R. Harris, Y. Kameda, R. Buchner, Y. Umebayashi, Possible proton conduction mechanism in pseudo-protic ionic liquids: A concept of specific proton conduction, J. Phys. Chem. B 123 (2019) 6244–6252.
[23] M. Aono, Y. Tomita, H. Abe, Y. Yoshimura, Nonequilibrium acidic fluctuations in room-temperature ionic liquid/water mixture: *N*, N-diethyl-N-methyl-N-(2-methoxyethyl)ammonium tetrafluoroborate, Chem. Lett. 41 (2012) 1532–1534.
[24] M. Aono, H. Abe, T. Takekiyo, Y. Yoshimura, Protonated/deprotonated properties of a room temperature ionic liquid–water system: *N*, *N*-Diethyl-*N*-methyl-*N*-2-methoxyethyl ammonium tetrafluoroborate, Chem. Phys. Lett. 598 (2014) 65–68.
[25] M. Aono, H. Abe, T. Takekiyo, Y. Yoshimura, Time and temperature dependences of electrochemical property in room temperature ionic liquids-water solutions: *N*, *N*-diethyl-*N*-methyl-*N*-2-methoxyethyl ammonium tetrafluoroborate, J. Jpn. Inst. Energy 93 (2014) 517–520.
[26] X. Cui, S. Zhang, F. Shi, Q. Zhang, X. Ma, L. Lu, Y. Deng, The influence of the acidity of ionic liquids on catalysis, ChemSusChem 3 (9) (2010) 1043–1047.
[27] R. Kanzaki, H. Kodamatani, T. Tomiyasu, H. Watanabe, Y. Umebayashi, A pH scale for the protic ionic liquid ethylammonium nitrate, Angew. Chem. Int. Ed. 55 (21) (2016) 6266–6269.
[28] H. Abe, K. Nakama, R. Hayashi, M. Aono, T. Takekiyo, Y. Yoshimura, K. Saihara, A. Shimizu, Electrochemical anomalies of protic ionic liquid – Water systems: A case study using ethylammonium nitrate – Water system, Chem. Phys. 475 (2016) 119–125.
[29] H. Abe, M. Aono, T. Takekiyo, Y. Yoshimura, A. Shimizu, Phase behavior of water-mediated protic ionic liquid: Ethylammonium nitrate, J. Mol. Liq. 241 (2017) 301–307.
[30] H. Abe, T. Takekiyo, Y. Yoshimura, A. Shimizu, S. Ozawa, Multiple crystal pathways and crystal polymorphs in protic ionic liquids, J. Mol. Liq. 269 (2018) 733–737.
[31] S. Ozawa, H. Kishimura, S. Kitahira, K. Tamatani, K. Hirayama, H. Abe, Y. Yoshimura, Isomer effect of propanol on liquid–liquid equilibrium in hydrophobicroom-temperature ionic liquids, Chem. Phys. Lett. 613 (2014) 122–126.
[32] H. Abe, R. Fukushima, M. Onji, K. Hirayama, H. Kishimura, Y. Yoshimura, S. Ozawa, Two-length scale description of hydrophobic room-temperature ionic liquid–alcohol systems, J. Mol. Liq. 215 (2016) 417–422.
[33] A.D. Becke, Density-functional thermochemistry. III. The role of exact exchange, J. Chem. Phys. 98 (1993) 5648–5652.
[34] C. Lee, W. Yang, R.G. Parr, Development of the Colle-Salvetti correlation-energy formula into a functional of the electron density, Phys. Rev. B 37 (2) (1988) 785–789.
[35] A.A. Granovsky, Firefly version 8, http://classic.chem.msu.su/gran/firefly/index.html.
[36] M.W. Schmidt, K.K. Baldridge, J.A. Boatz, S.T. Elbert, M.S. Gordon, J.H. Jensen, S. Koseki, N. Matsunaga, K.A. Nguyen, S. Su, T.L. Windus, M. Dupuis, J.A. Montgomery, General atomic and molecular electronic structure system, J. Comput. Chem. 14 (11) (1993) 1347–1363.
[37] E. Cancès, B. Mennucci, J. Tomasi, A new integral equation formalism for the polarizable continuum model: theoretical background and applications to isotropic and anisotropic dielectrics, J. Chem. Phys. 107 (1997) 3032–3041.
[38] A.E. Reed, L.A. Curtiss, F. Weinhold, Chem. Rev. 88 (1988) 899–926.
[39] T.L. Greaves, D.F. Kennedy, A. Weerawardena, N.M.K. Tse, N. Kirby, C.J. Drummond, Nanostructured protic ionic liquids retain nanoscale features in aqueous solution while precursor Brønsted acids and bases exhibit different behavior, J. Phys. Chem. B 115 (9) (2011) 2055–2066.
[40] X. Sun, B. Cao, X. Zhou, S. Liu, X. Zhu, H. Fub, Theoretical and experimental studies on proton transfer in acetate-based protic ionic liquids, J. Mol. Liq. 221 (2016) 254–261.
[41] R. Jacobi, F. Joerg, O. Steinhauser, C. Schröder, Emulating proton transfer reactions in the pseudo-protic ionic liquid 1-methylimidazolium acetate, Phys. Chem. Chem. Phys. 24 (2022) 9277–9285.
[42] S. Tsuzuki, K. Hayamizu, S. Seki, Y. Ohno, Y. Kobayashi, H. Miyashiro, Quaternary ammonium room-temperature ionic liquid including an oxygen atom in side chain/lithium salt binary electrolytes: Ab initio molecular orbital calculations of interactions between ions, J. Phys. Chem. B 112 (2008) 9914–9920.
[43] E. Bodo, M. Bonomo, A. Mariani, Assessing the structure of protic ionic liquids based on triethylammonium and organic acid anions, J. Phys. Chem. B 125 (2021) 2781–2792.